

Mesoscopics in Spintronics: Quantum Interference Effects in Spin-Polarized Electron Transport

Branislav K. Nikolić* and J. K. Freericks

Department of Physics, Georgetown University, Washington, DC 20057-0995

We generalize a Landauer-type formula, using a real \otimes spin-space Green function technique, to treat spin-dependent transport in quantum-coherent conductors attached to two ferromagnetic contacts. The formalism is employed to study the properties of components of an exact zero-temperature conductance matrix \mathbf{G} , as well as their mesoscopic fluctuations, describing injection and detection of a spin-polarized current in a two-dimensional system where electrons exhibit an interplay between Rashba spin-orbit (SO) coupling and phase-coherent propagation through a disordered medium. Strong Rashba coupling leads to a dramatic reduction of localization effects on the conductances and their fluctuations, whose features depend on the spin-polarization of injected electrons. In the limit of weak Rashba interaction antilocalization vanishes (i.e., the sum of the matrix elements of \mathbf{G} is almost independent of the SO coupling), but the partial spin-resolved conductances can still be non-zero. Besides spin-resolved conductance fluctuations and antilocalization, unusual quantum interference effects are revealed in this system leading to a negative difference between the partial conductances for a parallel and an antiparallel orientation of the contact magnetization, in a range of disorder strengths and for a particular spin-polarization of incoming electron with respect to the direction of Rashba electric field.

PACS numbers: 72.25.-b, 72.25.Rb., 73.23.-b, 85.75.Hh.

I. INTRODUCTION

Due to its fundamentally quantum nature, electron spin has very limited choice of interactions through which it can couple to the environment. Thus, its polarization can survive various forces in metals or semiconductors, while charge carriers undergo many scattering events, for long enough time to allow for envisioned quantum technologies that manipulate spin, such as spintronics^{1,2} or solid-state quantum computing with spin-qubits.³ Spintronic engineering of spin-polarized currents, combined with conventional electronics that manipulate electron charge, offers an exciting prospect to assemble information processing, storage, and communication on the same chip. Recent experimental advances have provided an impetus to study spin-polarized transport in two-dimensional electron systems, posing theoretical challenges⁴ where the ubiquitous “factor of two” for spin degeneracy in usual transport formulas has to be replaced by a more involved analysis of the interplay between orbital and spin degrees of freedom of the electrons.

While quantum-coherence of spin is essential for spintronic qubits, as well as some of the proposed spintronic devices for classical information processing,² modeling of the orbital kinetics of electrons that carry spin has mostly followed the traditional route of device engineering in charge-electronics: the charge transport (ballistic or diffusive) is described by a semiclassical Boltzmann formalism treating electrons and holes as classical particles where quantum effects enter only through their kinetic energy (being determined by the semiconductor band structure).^{5,6} Although many applications require devices operating at room temperature (where phase-coherence of orbital degrees of freedom is usually washed out), from the fundamental transport physics point of

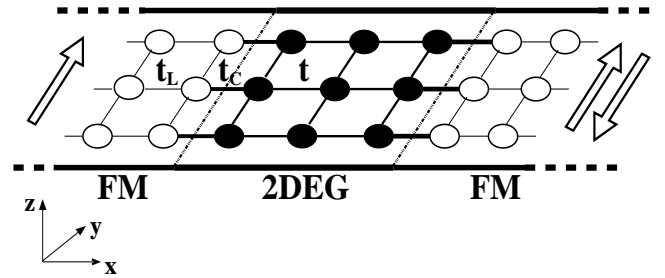


FIG. 1: Graphical depiction of our lattice model for a generic two-probe quantum spintronic FM-Sm-FM device: two ferromagnetic contacts (FM), that act as a spin injector (left) and a spin detector (right) are attached to a two-dimensional electron gas (e.g., in InAs), which is confined to the xy -plane by a Rashba electric field along the z -axis. The white arrows denote one possible magnetization configuration for the spin-resolved measurements (e.g., spin-up along y -axis is injected and both spins are collected). Each site hosts a single s -orbital which hops to four (or fewer for surface atoms) nearest neighbors. The hopping matrix element is t (within the sample), t_L (within the FM leads), and t_C (coupling of the sample to the leads). The leads are semi-infinite and connected smoothly at $\pm\infty$ to macroscopic reservoirs biased by the chemical potential difference $\mu_L - \mu_R = eV$.

view, it is intriguing to explore quantum interference effects involving both the charge and spin of the electrons in nanoscale samples at very low temperatures $\lesssim 1\text{K}$ —a playground of mesoscopic physics over the past two decades.⁷ Moreover, better understanding of the role of conserved quantum coherence of both wave functions and spin states in the conduction process is crucial for the devices that involve spin-polarized resonant tunneling.⁸ Recent theoretical efforts have been exploring mesoscopic aspects of spintronics by extending standard techniques

(such as, the Landauer-Büttiker scattering approach to quantum transport of *spinless* particles in finite-size systems^{9,10}) to describe transport in the presence of spin-dependent interactions by taking into account quantum-coherent dynamics of both orbital and spin degrees of freedom.^{4,11} Even though it is possible to add local spin-dependent effects into the scattering matrix directly, such extensions become highly non-trivial in the most general case where spin effects occur all over the system, as in the presence of SO interactions.^{4,12}

A particularly important interaction for semiconductor spintronics is the Rashba type of spin-orbit coupling,¹³ which is different from the more familiar impurity induced and position dependent one in metals.¹⁴ It arises from the asymmetry along the z -axis of the confining quantum well electric potential (generating a magnetic field in the electron rest frame) that creates a two-dimensional (2D) electron gas (xy -plane) on a narrow-gap semiconductor surface. Since the Rashba coupling can be tuned by an external gate electrode,¹⁵ it is envisaged as a tool to control the precession of the electron spin in the Datta-Das proposal for a field-effect spin transistor.² Thus, in such spin-interference devices intrinsic magnetic degrees of freedom can be controlled by electrical means. The spin-FET embodies a paradigm of a spintronic two-terminal device, such as the one shown in Fig. 1: **(i)** at the source (injector), information is stored as spins in a particular orientation (spin-up \uparrow or spin-down \downarrow); **(ii)** the spins, being attached to conduction electrons, carry the information along a non-magnetic sample where they are manipulated through spin-dependent interactions; and **(iii)** the information is read off at the drain (detector). The successful realization of such devices demands resolution of some of the paramount fundamental problems in current spintronic research: all-electrical injection, at *room temperature*, of fully spin-polarized currents into a semiconductor^{5,16} (on the same footing as demonstrated in metallic devices¹⁷ where large currents of cold-electrons can be injected and detected via Ohmic contacts); efficient spin detection at a drain electrode (spin measurement is impeded by the same feature that generates long coherence times making it technologically interesting—weak coupling to the environment¹⁸); and the engineering of spin-orbit couplings.¹⁵

The paper commences with the discussion of different types of quantum coherence that can be encountered in spintronic structures (Sec. II). These intuitive notions are then rigorously elaborated within the tensor product formalism for the joint description of spin and orbital quantum states, thereby making it easy to include effects of quantum coherence in the computation of transport quantities relevant for spintronics. The central such quantity is the conductance matrix \mathbf{G} describing spin-resolved transport measurements. We then introduce an efficient technique to compute \mathbf{G} by developing an implementation (based on lattice Green functions^{9,35} formulated in the tensor product of real and

spin space, rather than wave functions) of the Landauer-Büttiker formulation of linear response transport. Our formalism can accommodate both local and non-local effects of spin dynamics. We then reexamine in Sec. III the salient quantum interference effects of mesoscopic—conductance fluctuations and (anti)localization—for the matrix elements of \mathbf{G} , as well as their sums, corresponding to different spin-resolved measurements on a ferromagnet-semiconductor-ferromagnet (FM-Sm-FM) system where disorder is gradually increased in the central non-magnetic region. This allows us to sweep through different transport regimes: from ballistic (where few scattering events take place within the sample of size L since mean free path satisfies $\ell \gtrsim L$) to strongly disordered (where mean free path loses its meaning). Recent quantum-coherent treatments of spin-polarized transport in two-terminal devices have been confined to clean samples^{11,19} because the Datta-Das original spin-FET proposal (which has ignited much of the interest for semiconductor spintronics) requires strictly ballistic transport regime for the charge degrees of freedom. However, some level of scattering (from impurities, boundaries, or at the FM-Sm interface) is inevitable, and it is important to understand properties of spin-polarized injection, conduction, and degradation of well-defined spin-polarization in such environment.²⁰ For example, peculiar quantum interference effects, arising from the entanglement of spin and orbital degrees of freedom,^{4,26} are revealed in our disordered FM-Sm-FM system when analyzing the relationship between partial conductances (elements of \mathbf{G}) as a function of the Rashba SO coupling, disorder strength, and orientation of incoming electron spin with respect to the Rashba electric field (Sec. IV). We summarize our main findings in Sec. V.

II. HAMILTONIAN APPROACH TO QUANTUM SPIN-POLARIZED TRANSPORT

A. Quantum coherence within the tensor product formalism

In the general formalism of nonrelativistic quantum mechanics, spin degrees of freedom are internal, and are therefore described within a separate finite-dimensional vector space \mathcal{H}_s which has to be multiplied tensorially with an orbital space \mathcal{H}_o to get the *full* Hilbert space of quantum states $\mathcal{H} = \mathcal{H}_o \otimes \mathcal{H}_s$. Any operator acting in \mathcal{H} can be expressed as a linear combination of the tensor products $\hat{O}_o \otimes \hat{O}_s$, where \hat{O}_o and \hat{O}_s act in \mathcal{H}_o and \mathcal{H}_s , respectively. A generic Hamiltonian model for spintronics $\hat{H} = \hat{H}_o + \hat{H}_s + \hat{H}_{so}$ contains the following pieces: $\hat{H}_o \equiv \hat{O}_o \otimes \hat{I}_s$ which acts nontrivially in \mathcal{H}_o and like a unit operator \hat{I}_s in \mathcal{H}_s ; $\hat{H}_s \equiv \hat{I}_o \otimes \hat{O}_s$ acting nontrivially in \mathcal{H}_s ; and SO terms \hat{H}_{so} which are linear combinations of a tensor product of spin and orbital operators coupling the two spin-polarized subsystems. The advantage of spintronics modeling through a quantum transport formal-

ism that takes as an input a microscopic single-particle Hamiltonian is that spin, as a genuine quantum attribute of an electron, is treated in the most natural way by an operator acting in a two-dimensional vector space \mathcal{H}_s . The spin-dependent interactions are then accounted for by the terms in a Hamiltonian that are functions of the spin operator $\hat{\mathbf{S}} = \hbar\hat{\boldsymbol{\sigma}}/2$ [$\hat{\boldsymbol{\sigma}} = (\hat{\sigma}_x, \hat{\sigma}_y, \hat{\sigma}_z)$ is a vector of the Pauli spin matrices] acting in \mathcal{H}_s . An arbitrary state vector $|\Psi\rangle \in \mathcal{H}$ is a linear combination of the separable (i.e., uncorrelated) states forming a basis $|\phi_\alpha\rangle \otimes |\sigma\rangle$, where $|\phi_\alpha\rangle$ are basis states in \mathcal{H}_o and corresponding basis state $|\sigma\rangle$ in \mathcal{H}_s are the spin eigenstates $|\sigma\rangle$ of $\hat{\boldsymbol{\sigma}} \cdot \hat{\mathbf{u}}$ ($\sigma = \uparrow, \downarrow$ is a quantum number labeling the two eigenstates, and $\hat{\mathbf{u}}$ is a unit vector along the spin-quantization axis which is taken to be parallel to the magnetization of the ferromagnetic contacts in FM-Sm-FM geometry).

Most of quantum-interference phenomena observed in standard mesoscopic experiments (such as, weak localization, conductance fluctuations, or the Aharonov-Bohm effects⁷) probe the *orbital* quantum coherence of electron states, which requires preservation of the relative phase of linear superpositions of spatial states of the electron.⁷ Such mesoscopic systems are smaller than the dephasing length L_ϕ (typically $L_\phi \lesssim 1 \mu\text{m}$ at low enough temperatures $T \lesssim 1\text{K}$) set by inelastic processes. Thus, coherence times relevant for these investigations are completely disconnected from the spin coherence times T_2 over which the relative phase in superpositions of \uparrow and \downarrow spin states is well-defined³ (transport of phase-coherent spin states has been observed²¹ over length scale $L_2 \sim 100 \mu\text{m}$ in semiconductors at low temperatures where T_2 can reach 100 ns). For an ensemble of spins created in experiments²², the operational loss of phase coherence is described by the dephasing time T_2^* due to inhomogeneities in the Zeeman terms (although such dephasing is independent of individual spin decoherence, it provides experimentally measurable lower bound $T_2^* \leq T_2$). The other basic time scale which, together with T_2 , captures essential features of spin dynamics is the spin relaxation time T_1 (typically $T_1 \geq T_2$). The time T_1 is classical in nature since it determines lifetime of an excited spin state (aligned long the external magnetic field), i.e., the relaxation of unbalanced populations of spin states toward thermal equilibrium so that no concept of superpositions of quantum states is involved.²³ Corresponding spin diffusion length L_1 sets the upper limit to the size for any spintronic device since beyond this scale spin-encoded information completely fades away.²³ The principal interactions providing modes of decoherence and spin relaxation are exchange coupling with other electron (or nuclear) spins and SO coupling to impurity atoms and defects. In spintronic systems of current interest, one can encounter quantum interference effects stemming from spin coherence^{2,24}, both spin and orbital coherence that are independent of each other,⁸ or intertwined spin and orbital coherence when SO interaction are strong.²⁵

These different quantum-coherent situations become transparent after being recast in the formalism of tensor

products of Hilbert spaces and corresponding operators. In conventional *macroscopic* solids at finite temperatures one has to use a quantum statistical mechanics description of electrons in terms of density operators²⁷ (i.e., density matrices when a particular representation is chosen)

$$\hat{\rho}_{\text{macro}} = \hat{\rho}_o \otimes \hat{\rho}_s. \quad (1)$$

which are determined by thermal equilibrium. The most general quantum state of a spin- $\frac{1}{2}$ particle is accounted for by a density operator^{27,28}

$$\hat{\rho}_s = \frac{1}{2} \left(\hat{I}_s + \mathbf{p} \cdot \hat{\boldsymbol{\sigma}} \right), \quad (2)$$

where $0 \leq |\mathbf{p}| \leq 1$. For example, $|\mathbf{p}| = 1$ describes a pure quantum state which is fully *polarized* in the direction of vector \mathbf{p} , while $|\mathbf{p}| = 0$ stands for a non-pure state (the so-called *mixture*) that is completely unpolarized. The trivial example is injection of both spin states in equal proportion, $\hat{\rho}_s = 1/2 (|\uparrow\rangle\langle\uparrow| + |\downarrow\rangle\langle\downarrow|) = \hat{I}_s/2$. Coupling of electron spin to the environment of surrounding electronic or nuclear spins causes decoherence of spin quantum state, i.e., appearance of mixtures $|\mathbf{p}| < 1$ of spin states instead of a single pure state. In semiclassical spintronics, the spin part of the full (non-pure) state becomes a pure state $\hat{\rho}_s = |\Sigma\rangle\langle\Sigma|$. Then, after taking only diagonal elements of $\hat{\rho}_o$, a semiclassical description in terms of the Boltzmann distribution functions for \uparrow and \downarrow electrons is obtained where phase-relations between different states are ignored⁹ (as applicable to systems with $L > L_\phi$). Saying that the sample is *phase-coherent* in standard *mesoscopic* physics has a simple meaning in the formal language: an electron is described throughout the sample by a single wave function $\Phi(\mathbf{r}) = \langle \mathbf{r} | \Phi \rangle \in \mathcal{H}_o$, i.e., the orbital factor gets “purified” $\hat{\rho}_o = |\Phi\rangle\langle\Phi|$ at low enough temperatures where dephasing processes are suppressed below μm scales (while in usual experiments with unpolarized currents the spin factor is $\hat{\rho}_s = 1/2 \hat{I}_s$). In sample with both orbital and spin quantum coherence, the full state is pure $\hat{\rho}_{\text{meso}}^2 = \hat{\rho}_{\text{meso}}$, such as

$$\hat{\rho}_{\text{meso}} = |\Phi\rangle\langle\Phi| \otimes |\Sigma\rangle\langle\Sigma|, \quad (3)$$

The separability of the full state in Eq. (3) holds only when scattering events are spin-independent (such as those generated by lattice imperfections, phonons, and non-magnetic impurities), thereby leaving the spin state of a traversing electron unchanged. In this case, the orbital and spin factor states evolve independently in a coherent fashion within its own factor subspaces \mathcal{H}_s or \mathcal{H}_o , under the unitary operator generated by the corresponding Hamiltonian. However, in the presence of spin-orbit interaction, these two quantum-coherences become intertwined (note that if reduced density operator, obtained by tracing over the states in the other factor spaces, is pure, than it must be a factor of the total state operator²⁷). For example, if separable state with $|\uparrow\rangle$ spin factor is injected into a device with spin-orbit coupling, it will

evolve by unitary quantum evolution into a linear superposition $|\Psi_\uparrow\rangle$ of the separable state vectors $|\phi_\alpha\rangle \otimes |\sigma\rangle$ of some basis in \mathcal{H} . Such superpositions are still *pure*, albeit non-separable quantum states, i.e., the different degrees of freedom (orbital and spin) of one and the same particle have become *entangled*.²⁸ Thus, in this case individual spin or orbital states lose their coherence since they are not pure any more (although no real ensemble of different quantum states corresponding to such mixtures exists in the sample,²⁹ contrary to the case in the example of mixed spin states given above). This is analogous to the general decoherence mechanism that operates by entangling quantum system to its environment.²⁹ It also explains the formal meaning of ‘spin-orbit quantum interference effects’,²⁵ since entanglement is entailed by linear superpositions of states in the full Hilbert space \mathcal{H} . Moreover, such entangled states display quantum-mechanical non-locality, usually studied in the context of entanglement of two particles (e.g., Einstein-Podolsky-Rosen or Bell states²⁷), which manifests here as “wholistic” spin effects all throughout the system.¹² When both \uparrow and \downarrow particles are injected, the state of an electron is a statistical superposition $|\Psi_\uparrow\rangle\langle\Psi_\uparrow| + |\Psi_\downarrow\rangle\langle\Psi_\downarrow|$, rather than the coherent one $|\Psi_\uparrow\rangle + |\Psi_\downarrow\rangle$. Thus, the quest for spintronic devices that would utilize quantum-coherent dynamics of all degrees of freedom requires to master the control of spins without destroying the phase coherence of orbital degrees of freedom⁸ (as is the case when many-body interactions with surrounding nuclear spins or other electrons³⁰ are involved), and *vice versa*.²⁵

The effects of quantum-coherence on electronic transport are most easily discussed within the Landauer-Büttiker scattering approach. To study spin-polarized quantum transport, the basis of asymptotic scattering states at the Fermi energy E_F in the leads should be comprised of the following vectors

$$\langle\mathbf{r}|p\rangle_\sigma^\pm = \Phi_p(y) \otimes \exp(\pm ik_p x) \otimes |\sigma\rangle. \quad (4)$$

In the spinless case, the orbital factors are usually referred to as conducting ‘channels’¹⁰; here a ‘spin-polarized channel’ $p\sigma$ has a real wave number $k_p > 0$, a transverse wave function $\Phi_p(\mathbf{r})$ defined by quantization of transverse momentum in the leads of finite cross section and given boundary conditions, and a spin factor state $|\uparrow\rangle$ or $|\downarrow\rangle$. Thus, injecting a flux concentrated in the channel $|\text{in}\rangle \equiv |p\rangle \otimes |\sigma\rangle$ will generate the following quantum state in the opposite lead

$$|\text{out}\rangle = \sum_{q,\sigma'} \mathbf{t}_{qp,\sigma'\sigma} |q\rangle \otimes |\sigma'\rangle. \quad (5)$$

In the most general situation, with spin-dependent charge scattering present in the central region, this state is coherent mixture of all spin-polarized channels (4). This equation introduces a transmission matrix \mathbf{t} , whose elements are $\mathbf{t}_{qp,\sigma'\sigma}$. The \mathbf{t} -matrix accounts for the unitary transformation that the central region would perform on the incoming electronic wave function from the left lead.

The formalism we introduce here is capable of dealing with all of the variety of quantum-coherent situations relevant for transport (i.e., coherent superpositions of scattering quantum states in \mathcal{H}_o , \mathcal{H}_s , or $\mathcal{H}_o \otimes \mathcal{H}_s$) in arbitrary geometry, and for arbitrary values of interaction strengths, as long as one stays within the domain of single-particle picture. We choose the Anderson model for \hat{H}_o (which is often used for numerical modeling of quantum transport,⁹ localization-delocalization transition,³¹ and brute force computation of conductance fluctuations,^{32,33})

$$\hat{H}_o = \left(\sum_{\mathbf{m}} \varepsilon_{\mathbf{m}} |\mathbf{m}\rangle\langle\mathbf{m}| + \sum_{\langle\mathbf{m},\mathbf{n}\rangle} t_{\mathbf{m}\mathbf{n}} |\mathbf{m}\rangle\langle\mathbf{n}| \right) \otimes \hat{I}_s, \quad (6)$$

on a square $N \times N$ lattice ($L = Na$, with a being the lattice spacing). Here $t_{\mathbf{m}\mathbf{n}} = te^{2\pi i\phi_{\mathbf{m}\mathbf{n}}}$, t is the nearest-neighbor hopping integral between s -orbitals $\langle\mathbf{r}|\mathbf{m}\rangle = \psi(\mathbf{r} - \mathbf{m})$ on adjacent atoms located at sites $\mathbf{m} = (m_x, m_y)$ of the lattice. The *local orbital basis* is advantageous since it allows one to treat an *arbitrary* measurement geometry, which is an essential ingredient in the studies of quantum transport through finite-size mesoscopic systems.³⁴ In the applied magnetic field, the link fields $\phi_{\mathbf{m}\mathbf{n}} = -\phi_{\mathbf{n}\mathbf{m}}$ entering the Peierls phase factor introduce Aharonov-Bohm phases into the tight-binding model so that the flux through a given loop S is $\Phi_S = \sum_{\langle\mathbf{m},\mathbf{n}\rangle \in S} \phi_{\mathbf{m}\mathbf{n}}$ in units of the flux quantum h/e . The disorder is simulated by taking a random on-site potential with $\varepsilon_{\mathbf{m}}$ being uniformly distributed over the interval $[-W/2, W/2]$ [the other possibilities to introduce disorder is random hopping, $t \in [1 - 2W, 1]$, or random fluxes $\phi_{\mathbf{m}\mathbf{n}} \in [0, 2\pi]$]. The lattice site states of \hat{H}_o multiplied tensorially by $|\sigma\rangle$ define a basis $|\mathbf{m}\rangle \otimes |\sigma\rangle$ in \mathcal{H} , and therefore a real \otimes spin-space representation of the operators in our algorithm.

The purely spin part of \hat{H} is exemplified by a Zeeman term

$$\hat{H}_s = -\hat{I}_o \otimes \mu \hat{\boldsymbol{\sigma}} \cdot \mathbf{B}, \quad (7)$$

where $\mu = g^* \mu_B / 2$ (g^* is an effective gyromagnetic ratio and μ_B is the Bohr magneton) and \mathbf{B} is the applied magnetic field. Finally, the relevant SO couplings in 2D heterostructures⁴⁰ (neglecting $\propto v^3$ terms) are given by the Rashba term¹³ $\alpha_R m^* (\hat{\boldsymbol{\sigma}} \times \hat{\mathbf{v}}) \cdot \hat{\mathbf{z}} / \hbar$ ($\hat{\mathbf{z}}$ is a unit vector orthogonal to the plane of the sample and m^* is the effective mass), and the Dresselhaus term⁴⁰ $\eta m^* (\hat{v}_x \hat{\sigma}_x - \hat{v}_y \hat{\sigma}_y) / \hbar$ (generated by the lack of inversion symmetry of a periodic crystal potential in the bulk, like in GaAs):

$$\begin{aligned} \hat{H}_{\text{so}} = & \frac{\alpha_R \hbar}{2a^2 t} (\hat{v}_x \otimes \hat{\sigma}_y - \hat{v}_y \otimes \hat{\sigma}_x) \\ & - \frac{\eta \hbar}{2a^2 t} (\hat{v}_x \otimes \hat{\sigma}_x - \hat{v}_y \otimes \hat{\sigma}_y), \end{aligned} \quad (8)$$

where we replace m^* by its tight-binding description in terms of $t = -\hbar^2 / 2m^* a^2$. The explicit use of the tensor-product notation in our formulas makes it possible to

obtain quickly and efficiently their matrix representation in a chosen basis. For example, to obtain the site-spin representation of the Rashba term in Eq. (8) we use the fact that velocity operator is a matrix

$$\langle \mathbf{m} | \hat{v}_x | \mathbf{n} \rangle = \frac{i}{\hbar} t_{\mathbf{m}\mathbf{n}} (m_x - n_x), \quad (9)$$

in the site representation, and then multiply, in the sense of direct product of matrices (when particular representation is chosen, \otimes stands for the Kronecker or direct product of matrices), this matrix with respective Pauli matrix. Thus, the final matrix elements in Eq. (8) are just dimensionless constants multiplied by the material-specific ‘‘spin-orbit hopping parameters’’ $t_{\text{so}}^{\text{R}} = \alpha_{\text{R}}/2a$ and $t_{\text{so}}^{\text{D}} = \eta/2a$ that set the energy scales of the Rashba and Dresselhaus terms, respectively.

The Rashba term added to the tight-binding Hamiltonian (6) will cause spin splitting [i.e., lifting of spin degeneracy for \uparrow and \downarrow states having the same momentum, $\mathbf{k} = (k_x, k_y) \neq 0$] of an energy subband of 2DEG into two branches

$$\begin{aligned} E(k_x, k_y) &= E_0(k_x, k_y) \pm \Delta E(k_x, k_y) \\ &= \varepsilon + 2t[\cos(k_x a) + \cos(k_y a)] \\ &\quad \pm 2t_{\text{so}}^{\text{R}} \sqrt{\sin^2(k_x a) + \sin^2(k_y a)}, \end{aligned} \quad (10)$$

for clean sample with constant ε on the diagonal [the splitting becomes linear¹¹ in the momentum $\Delta E = 2\alpha_{\text{R}}\sqrt{k_x^2 + k_y^2}$ for parabolic subband dispersion $E_0(k_x, k_y) = \hbar(k_x^2 + k_y^2)/2m^*$ characterizing continuous systems]. Such splitting of the conduction band as a result of spin-orbit coupling in the presence of an asymmetric confinement potential makes it a useful tool to model the electronic structure of confined narrow-gap semiconductors. Rashba SO term also induces, when viewed within the semiclassical picture, spin precession around effective Rashba magnetic field $\mathbf{B}_R(\mathbf{k})$ [Rashba Hamiltonian, like any SO term, can be interpreted as the interaction of electron spin with \mathbf{k} -dependent internal effective magnetic field, $\mathbf{B}(\mathbf{k}) \cdot \hat{\mathbf{S}}$] with frequency $\omega = \Delta E/2\hbar$. In the presence of disorder, the precession around $\mathbf{B}(\mathbf{k})$ for a given \mathbf{k} terminates after scattering of impurity (the other sources of scattering that change \mathbf{k} are boundary surface and phonons). Then it starts again but along a different randomly selected axis, so that the change of spin direction by full precession, which occurs in ballistic systems,^{2,11} is suppressed by disorder. In the cases of our study where interplay of the Rashba interaction and charge scattering takes place (at zero temperature), initial full polarization of injected electrons is destroyed (technically, measurement of the spin-dependent properties alone requires to use reduced density operator, which does not describe a pure state any more). This is analogous to D’yakonov-Perel’ mechanism,⁴¹ which is usually discussed in the context of spin relaxation²³, but in our study of transport through mesoscopic spintronics structures, which are effectively at zero-temperature, it is responsible for the spin decoherence.²⁸

B. Landauer-type conductance formula for quantum spin-polarized transport

The central result of our formalism is a direct algorithm to compute exactly the zero-temperature conductance matrix⁴ of a single sample

$$\mathbf{G} = \begin{pmatrix} G^{\uparrow\uparrow} & G^{\uparrow\downarrow} \\ G^{\downarrow\uparrow} & G^{\downarrow\downarrow} \end{pmatrix} = \frac{e^2}{h} \mathbf{T} = \frac{e^2}{h} \begin{pmatrix} T^{\uparrow\uparrow} & T^{\uparrow\downarrow} \\ T^{\downarrow\uparrow} & T^{\downarrow\downarrow} \end{pmatrix}, \quad (11)$$

We imagine that the 2D sample is attached via perfect Ohmic contacts (which are desirable but are currently problematic to achieve at FM-Sm interface together with efficient injection¹⁶) to two ideal semi-infinite leads (Fig. 1) where one serves to inject spin-polarized current from ferromagnetic contacts (emitting \uparrow or \downarrow electrons) into a semiconductor or nonmagnetic metal,³⁶ and the other one drains electrons to the contacts detecting \uparrow and/or \downarrow electrons. The leads also define, by transverse quantization, the orbital part of an asymptotic scattering state in Eq. (4). Moreover, they effectively remove ‘‘hot’’ electrons from the open sample, thereby bypassing the intricate issues of dissipation which must occur somewhere in the circuit to reach the steady-state regime under external pumping. While the trick of using ideal semi-infinite leads is a standard one in mesoscopic transport theory,⁹ the polarization of the asymptotic states stems from the different densities of states for \uparrow and \downarrow electrons in the ferromagnetic contacts (which can be conventional metallic or semiconducting, currently available only at low temperature³⁷). The meaning of \mathbf{G} is elucidated by casting it into a form analogous to the Landauer formula,^{9,10} where the usual sum of the transmission probabilities over all transverse propagating modes for spinless particles $T = \text{Tr} \mathbf{t} \mathbf{t}^\dagger$ is replaced by a 2×2 matrix \mathbf{T} of partial transmission coefficients describing the transition between left and right subsystems comprised of the two types \uparrow, \downarrow of spin-polarized asymptotic states.⁴ Thus, $T^{\uparrow\uparrow}$ is the sum of transmission probabilities, over all conducting channels, for \uparrow electron to travel from the left to the right lead whose magnetic moments are oriented in parallel. Analogously, $T^{\uparrow\downarrow}$ quantifies the probability to detect (in the setup with antiparallel magnetic moments of the contacts) \downarrow -electron arising from spin precession^{2,11} or spin-flips⁴ of the injected \uparrow -electrons.

Diagonal components of \mathbf{G} , $G^{\uparrow\uparrow}$ and $G^{\downarrow\downarrow}$, are familiar from the studies of giant-magnetoresistance³⁸ (in the case of spin-degenerate transport, trivially, $G^{\uparrow\uparrow} = G^{\downarrow\downarrow}$ and $G^{\uparrow\downarrow} = G^{\downarrow\uparrow} = 0$). On the other hand, properties of the off-diagonal ‘‘mixing’’ conductances, $G^{\uparrow\downarrow}$ and $G^{\downarrow\uparrow}$, are much less explored (also, for some problems of partially polarized transport between non-collinear ferromagnets they have been introduced recently as complex quantities³⁹). The \mathbf{G} -matrix allows one to compute the measured conductance in different setups for spin-resolved experiments

$$G_{\text{measured}} = \mathbf{s}_i^\dagger \cdot \mathbf{G} \cdot \mathbf{s}_c, \quad (12)$$

where \mathbf{s}_i , \mathbf{s}_c are vectors describing the type of incoherent mixture of \uparrow or \downarrow electrons which are injected or collected, respectively. This quantum conductance expression can also be employed to get results of semiclassical spintronics by taking a disorder average and the semiclassical approximation in the large system limit, as has been the practice in related giant-magnetoresistance studies of the transport with two independent ‘spin-channels’.³⁸

The conductance matrix Eq. (11) is calculated by generalizing a two-probe Landauer-type formula for the spin-degenerate transport, which is obtained in the linear-response and zero-temperature limit of an expression derived by the Keldysh technique,^{42,43} to a separate treatment of the two spin-polarized components

$$\mathbf{G} = \frac{e^2}{h} \sum_{i,j=1}^N \begin{pmatrix} |\mathbf{t}_{ij,\uparrow\uparrow}|^2 & |\mathbf{t}_{ij,\uparrow\downarrow}|^2 \\ |\mathbf{t}_{ij,\downarrow\uparrow}|^2 & |\mathbf{t}_{ij,\downarrow\downarrow}|^2 \end{pmatrix}, \quad (13a)$$

$$\mathbf{t} = 2\sqrt{-\text{Im} \hat{\Sigma}_L \otimes \hat{I}_s \cdot \hat{G}_{1N}^r \cdot \sqrt{-\text{Im} \hat{\Sigma}_R \otimes \hat{I}_s}}, \quad (13b)$$

The partial summation adds squared amplitudes of all elements of the transmission matrix \mathbf{t} having the same spin indices

$$\mathbf{t}_{ij,\uparrow\uparrow} \equiv \mathbf{t}_{2(i-1)+1,2(j-1)+1}, \quad (14a)$$

$$\mathbf{t}_{ij,\uparrow\downarrow} \equiv \mathbf{t}_{2(i-1)+1,2j}, \quad (14b)$$

$$\mathbf{t}_{ij,\downarrow\uparrow} \equiv \mathbf{t}_{2i,2(j-1)+1}, \quad (14c)$$

$$\mathbf{t}_{ij,\downarrow\downarrow} \equiv \mathbf{t}_{2i,2j}, \quad (14d)$$

where $i, j = 1, \dots, N$. Here $-\text{Im} \hat{\Sigma}_{L,R} = -(\hat{\Sigma}_{L,R}^r - \hat{\Sigma}_{L,R}^a)/2i$ are nonnegative matrices with a well-defined matrix square root, where $\hat{\Sigma}_{L,R}^a = [\hat{\Sigma}_{L,R}^r]^\dagger$ are the self-energies (r -retarded, a -advanced) describing the ‘‘interaction’’ of a sample with the left (L) or right (R) lead. The $2N \times 2N$ submatrix \hat{G}_{1N}^r of the full Green function matrix $\hat{G}_{\mathbf{nm},\sigma\sigma'}^r = \langle \mathbf{n}, \sigma | \hat{G}^r | \mathbf{m}, \sigma' \rangle$ connects the layers (i.e., rows of sites) 1 and N along the direction of transport (x -axis). The Green function, describing the propagation of \uparrow or \downarrow electron between two arbitrary sites inside an open conductor in the absence of inelastic processes, is the site-spin representation of the Green operator obtained by inverting the Hamiltonian for the given boundary conditions (hard wall in our case)

$$\hat{G}^r = [E\hat{I}_o \otimes \hat{I}_s - \hat{H} - \hat{\Sigma}^r \otimes \hat{I}_s]^{-1}, \quad (15)$$

where $\hat{\Sigma}^r = \hat{\Sigma}_L^r + \hat{\Sigma}_R^r$. The self-energy matrices introduced by the leads are non-zero only on the end layers of the sample adjacent to the leads. Their analytical form is known exactly as $\hat{\Sigma}_{L,R}^r(\mathbf{n}, \mathbf{m}) = t_C^2 \hat{g}_{L,R}^r(\mathbf{n}_S, \mathbf{m}_S, t_L)$, with $\hat{g}_{L,R}^r(\mathbf{n}_S, \mathbf{m}_S, t_L)$ the surface Green function of the bare semi-infinite lead between the sites \mathbf{n}_S and \mathbf{m}_S in the end atomic layer of the lead (adjacent to the corresponding sites \mathbf{n} and \mathbf{m} inside the conductor).^{9,35} Here t_L and t_C are the hopping parameters in the lead and on the lead-sample interface, respectively (see Fig. 1).

Although Eq. (13) assumes dynamics of noninteracting quasiparticles, it is also valid for the zero-temperature linear-response regime of an interacting system⁴³ (only single-electron elastic processes are allowed in this regime due to the requirements of energy conservation). In the scattering picture of transport of noninteracting quasiparticles on the tight-binding lattice, the orbital factor of the asymptotic states Eq. (4) is comprised of a quantized transverse wave function and a Bloch state (instead of a plane wave), where the corresponding dispersion relation is defined by the semi-infinite tight-binding lattice modeling the leads.³⁵ Since the Rashba electric field selects a preferred direction in space, one has to take into account the relative spin orientation of the incoming electron with respect to the z -axis. We choose the representation for the spin-part of the scattering state in Eq. (4) as $|\uparrow\rangle \rightarrow \begin{pmatrix} 1 \\ 0 \end{pmatrix}$ and $|\downarrow\rangle \rightarrow \begin{pmatrix} 0 \\ 1 \end{pmatrix}$. Therefore, the direction of the spin-polarization of injected and collected electrons is defined by specifying the direction for which spin-operator is diagonal. For example, to study the injection of particles that are spin-polarized along x -, y - and z - axis, we change the representation of the Pauli spin operators. For \uparrow, \downarrow along the z -axis

$$\hat{\sigma}(Z) = \left[\begin{pmatrix} 0 & 1 \\ 1 & 0 \end{pmatrix}, \begin{pmatrix} 0 & -i \\ i & 0 \end{pmatrix}, \begin{pmatrix} 1 & 0 \\ 0 & -1 \end{pmatrix} \right], \quad (16)$$

the usual textbook representation, where $\hat{\sigma}_z$ is diagonal, is used; for spin-polarization in the y -direction

$$\hat{\sigma}(Y) = \left[\begin{pmatrix} 0 & -i \\ i & 0 \end{pmatrix}, \begin{pmatrix} 1 & 0 \\ 0 & -1 \end{pmatrix}, \begin{pmatrix} 0 & 1 \\ 1 & 0 \end{pmatrix} \right], \quad (17)$$

and for spin-polarization along the x -axis

$$\hat{\sigma}(X) = \left[\begin{pmatrix} 1 & 0 \\ 0 & -1 \end{pmatrix}, \begin{pmatrix} 0 & -i \\ i & 0 \end{pmatrix}, \begin{pmatrix} 0 & -1 \\ -1 & 0 \end{pmatrix} \right]. \quad (18)$$

Note that only the diagonal matrix is unique, while the other two matrices are affected (as demonstrated here via one particular choice) by the freedom in choosing phase factors of eigenvectors forming the columns of unitary matrices \hat{U} which transform the standard set of Pauli matrices into a new diagonal representation $\hat{U}^\dagger \hat{\sigma} \hat{U}$ (therefore, it is more appropriate to talk about Pauli spin algebra whose operators satisfy abstract set of rules²⁷). The injection of electrons which are spin-polarized in the direction of transport (x -axis) and precess within the central region is a standard set-up of the spin-FET proposal. On the other hand, injecting y -axis (Fig 1) polarized electrons, whose spin is conserved throughout the semiconductor, corresponds to spin valves.¹⁹

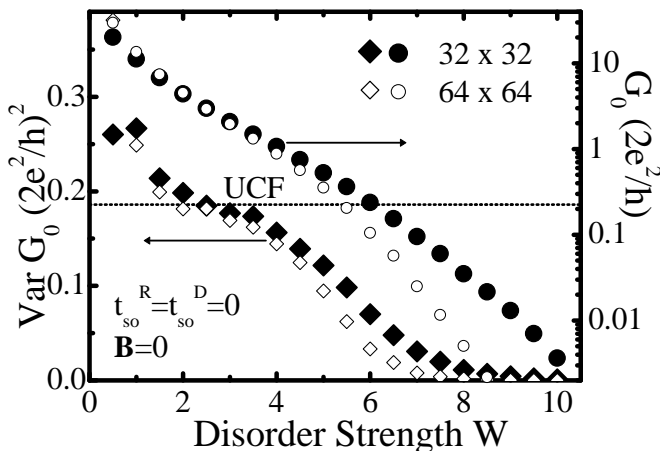


FIG. 2: Conductance G_0 (circles) and its variance $\text{Var } G_0$ (diamonds) in a time-reversal ($\mathbf{B}=0$) and spin-rotation invariant ($t_{\text{so}}^{\text{R}} = t_{\text{so}}^{\text{D}} = 0$) 2D conductor modeled on 32×32 or 64×64 half-filled ($E_F = 0$) tight-binding lattice as a function of disorder strength W (disorder-averaging is performed over 10000 samples). The dotted line is the value of the universal conductance fluctuations predicted perturbatively^{32,45} for the metallic diffusive regime.

III. CONDUCTANCE FLUCTUATIONS AND ANTILOCALIZATION OF SPIN-POLARIZED ELECTRONS IN DISORDERED RASHBA SPIN-SPLIT ELECTRON SYSTEM

A major boost for the development of mesoscopic physics came from the pioneering experimental⁴⁴ and theoretical^{32,45} studies of unexpectedly large conductance fluctuations (CF), $\text{Var } G \sim (e^2/h)^2$. Each phase-coherent sample is characterized by a fingerprint of reproducible (time-independent) conductance fluctuations as a function of magnetic field, Fermi energy, or change of impurity configuration at a fixed E_F . This violates the traditional notion that a given sample is well described by average values of physical quantities, particularly when $\text{Var } G$ becomes of the same order as $\langle G \rangle$ [\dots] denotes disorder averaging] as L approaches the localization length ξ . Thus, even in metals, CF scale as $\text{Var } G / \langle G \rangle^2 \sim L^{4-2d}$ in d -dimensions. Such counterintuitive behavior of CF and lack of self-averaging (especially in low-dimensional systems $d \leq 2$) necessitated the development of a “mesoscopic approach” as an alternative to standard statistical mechanics description of macroscopic condensed matter systems, where whole distribution functions of physical quantities are to be studied in nanoscale quantum-coherent solids containing a macroscopically large number of particles.⁷ In diffusive ($\ell \ll L \ll \xi$) metallic ($G \gg e^2/h$) conductors, CF are considered to be universal (UCF), $\text{Var } G = C_d(2e^2/h)^2$, where C_d is a constant independent of the sample size or the degree of disorder,¹⁰ at least within certain limits (C_d is reduced by a factor of 2, 4, or 8 by breaking time-reversal or spin-rotation invariance, or both,¹⁰ for an exhaustive list of symme-

try classes and possible crossovers in weakly disordered quantum dots and for weak SO coupling, see Ref. 48). However, numerical studies³³ of the evolution of $\text{Var } G$ in 3D mesoscopic metals show that CF monotonically decay with increasing disorder strength, becoming close to a constant predicted by the perturbative UCF theory^{32,45} only in a narrow range of W . Therefore, to have a reference point for the subsequent study of fluctuations of \mathbf{G} , we first calculate $\text{Var } G_0$ in the crossover between small and large W (i.e., from a quasiballistic, to a diffusive, and finally localized transport regime) for a conductor described by the non-interacting and spin-independent Hamiltonian \hat{H}_0 with $\mathbf{B} = 0 = \phi_{\text{mn}}$. The localization length in the band center $E_F = 0$ of the paradigmatic Anderson model (6) is³¹ $\xi \simeq (1 + 5.2 \cdot 10^4/W^4)a$, while its mean free path at the same Fermi energy is given by $\ell \simeq 30a(t/W)^2$. In this case, spin-degeneracy gives $G_0 = G^{\uparrow\uparrow} + G^{\downarrow\downarrow} = 2G^{\uparrow\uparrow}$ ($G^{\uparrow\downarrow} = G^{\downarrow\uparrow} = 0$). The result plotted in Fig. 2 demonstrates that $\text{Var } G_0$ decreases systematically with increasing $W \in [0, 10]$, while $C_2 = 0.186$ is the expected UCF value in 2D “metals” in the diffusive regime³² (in the quasiballistic regime CF are not expected to be universal⁴⁶).

A recent experimental investigation⁴⁷ of transport through open ballistic (but chaotic due to the surface scattering) quantum dots in a GaAs heterostructure, that are exposed to a large in-plane magnetic field, point to the emergence of a Rashba SO interaction as the essential ingredient in analyzing their CF.^{40,48} Inspired by their unexpected findings on the reduction of CF, we undertake a similar but spin-resolved analysis when spin-polarized electrons are injected into a 2D disordered open quantum dot. Thus, we “create” an experiment on the computer “measuring” the components of \mathbf{G} for each realization of disorder, and thereby sample-to-sample fluctuations $\text{Var } G_{\alpha\beta} = \langle G_{\alpha\beta}^2 \rangle - \langle G_{\alpha\beta} \rangle^2$ as a function of the disorder strength W and Rashba spin-orbit hopping parameter t_{so}^{R} . Since the Rashba SO coupling can be tuned in principle by an interface electric field,¹⁵ we sweep t_{so}^{R} (and neglect t_{so}^{D}) from the weak $t_{\text{so}}^{\text{R}} = 0.01$ to the strong $t_{\text{so}}^{\text{R}} = 1.0$ SO interaction limit⁴⁹ (a similar range of Rashba hopping has been explored for spin-polarized transport through clean wires where it was shown that even in the ballistic case, subbands in Eq. 10 defined by the orbital factor states can be mixed depending on the strength of the Rashba coupling and wire width¹¹). The important parameters to keep in mind are: $t_{\text{so}}^{\text{R}}/W$; the ratio ℓ/L which delineates boundaries of different transport regimes in the crossover from ballistic $\ell/L \gg 1$ to diffusive $\ell/L \ll 1$ transport (e.g., the diffusive transport regime can be reached at much weaker disorder but in very large sample, while the interplay of coherent scattering off impurities and spin-dependent interactions is the pronounced when the energy scale of the terms in \hat{H} introduced by \hat{H}_s and \hat{H}_{so} are comparable to the strength of the disorder); and ξ/L since for $\xi/L < 1$ electrons become localized.

The mesoscopic fluctuating properties of the compo-

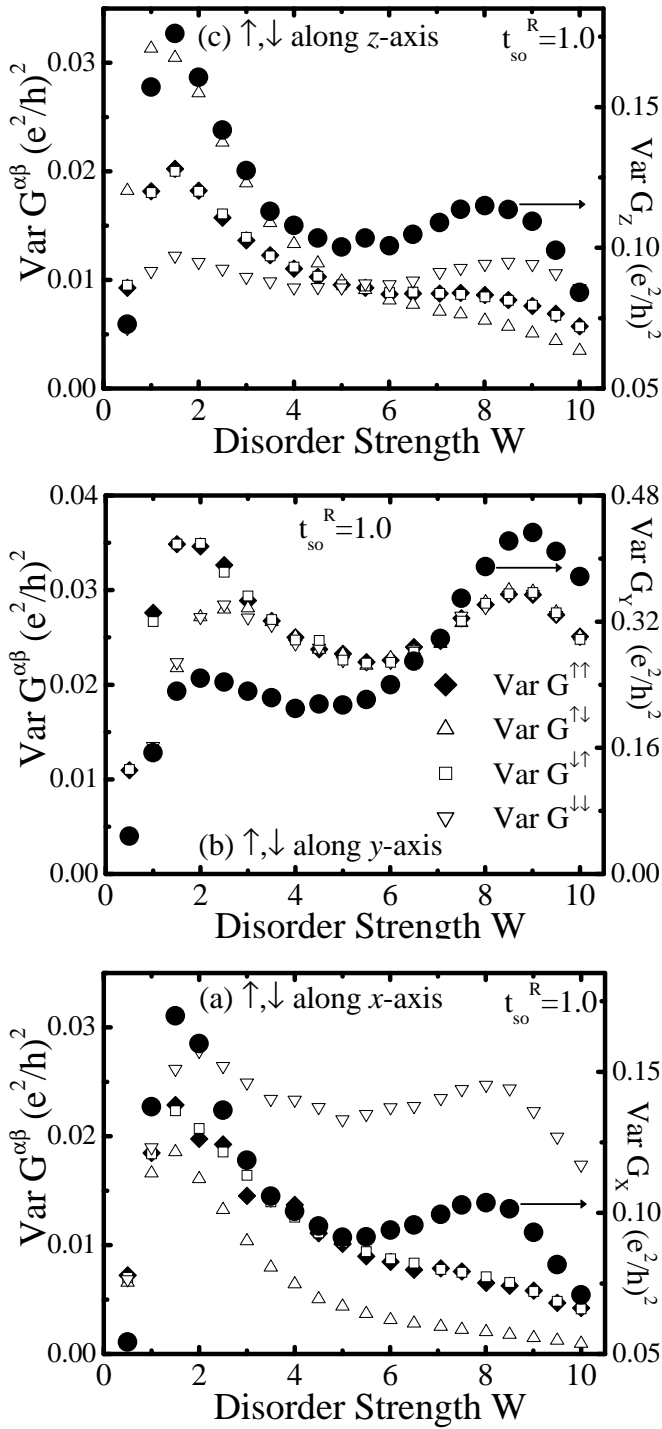


FIG. 3: Zero-temperature sample-to-sample fluctuations of the components of \mathbf{G} for transport which is spin-polarized \uparrow, \downarrow along: (a) the x -axis, (b) the y -axis, and (c) the z -axis. The 10000 samples are modeled on a 32×32 half-filled ($E_F = 0$) tight-binding lattice with diagonal disorder and a strong $t_{so}^R = 1.0$ Rashba SO coupling. The circles on all three panels are conductance fluctuations of the sum of the components of \mathbf{G} , e.g., $\text{Var} G_Z = \text{Var}[G^{\uparrow\uparrow} + G^{\downarrow\downarrow} + G^{\uparrow\downarrow} + G^{\downarrow\uparrow}]$, which describes injection and detection of both spin species polarized in the x -, y - or z -direction for $\text{Var} G_X$, $\text{Var} G_Y$, and $\text{Var} G_Z$, respectively.

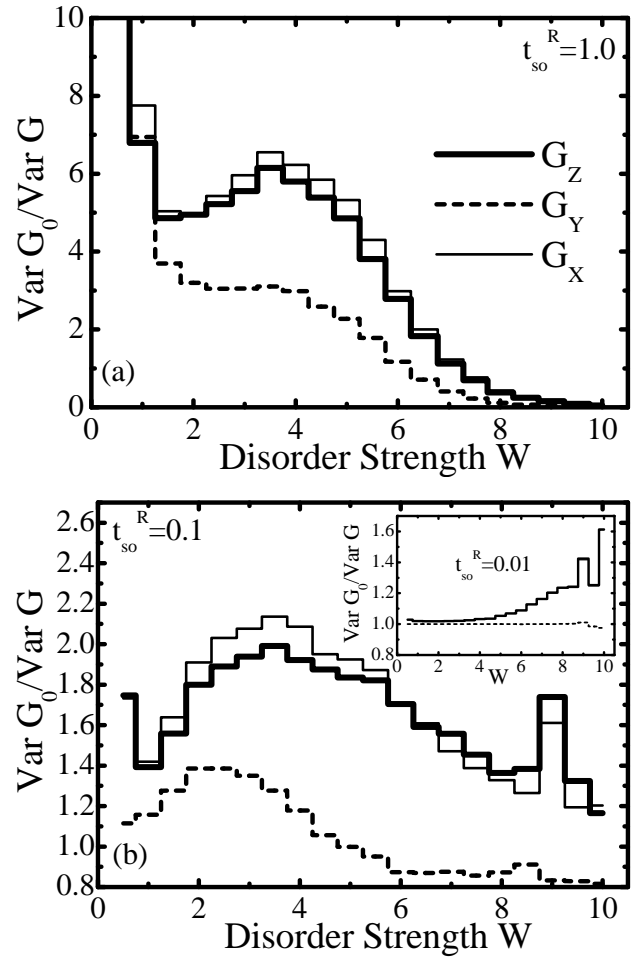


FIG. 4: Ratio $\text{Var} G_0 / \text{Var} G$ of the conductance fluctuations in a pure disordered case (Fig. 2) to the fluctuations of the sums of the elements of \mathbf{G} ($G \equiv G_X, G_Y$, and G_Z) from Fig. 3. This reduction factor due to the Rashba interaction is plotted for: (a) the strong SO coupling limit $t_{so}^R = 1.0$; and (b) the weak SO coupling limit $t_{so}^R = 0.1$ or 0.01 .

nents of \mathbf{G} , for FM magnetization lying \uparrow, \downarrow in the x -, y - and z -direction, are shown in Fig. 3 for the largest $t_{so}^R = 1.0$. The complete suppression of CF in the weakest disorder case (standard conductance fluctuations reach a maximum in the quasiballistic transport regime,⁴⁶ as shown in Fig. 2) is a feature of the strong SO coupling limit. While $\text{Var} G^{\uparrow\uparrow} \approx \text{Var} G^{\downarrow\downarrow}$ in all cases, fluctuations of the off-diagonal partial conductances $\text{Var} G^{\uparrow\downarrow}$ and $\text{Var} G^{\downarrow\uparrow}$ can display quite different patterns and even be independent of the disorder strength (“universality”), unlike the case of G_0 or the total conductances G_X, G_Y, G_Z introduced below.

The counterpart of the measured conductance in experiments on unpolarized electrons⁴⁷ would be to inject and collect both pure spin states $\mathbf{s}_i = \mathbf{s}_c = \begin{pmatrix} 1 \\ 1 \end{pmatrix}$:

$$G = \mathbf{s}_i^\dagger \cdot \mathbf{G} \cdot \mathbf{s}_c = G^{\uparrow\uparrow} + G^{\uparrow\downarrow} + G^{\downarrow\uparrow} + G^{\downarrow\downarrow}. \quad (19)$$

Therefore, Fig. 3 also plots the CF properties of the total

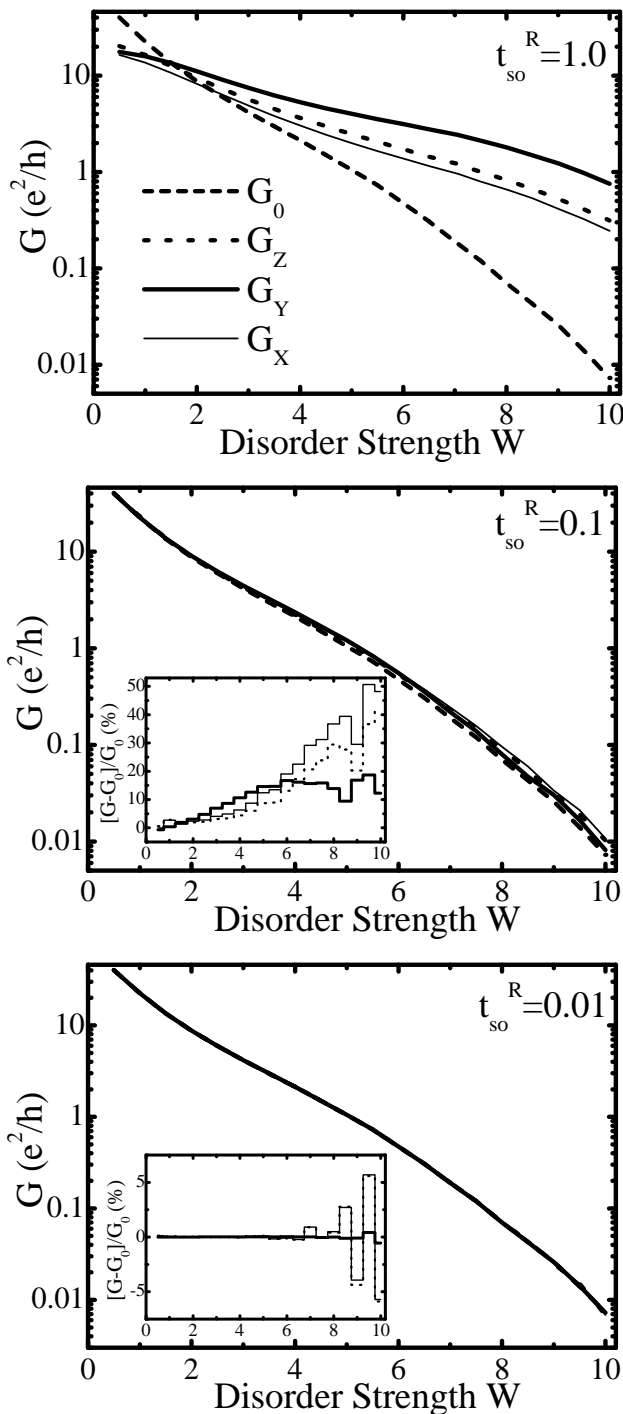


FIG. 5: The total conductance $G_{X,Y,Z} = G^{\uparrow\uparrow} + G^{\downarrow\downarrow} + G^{\uparrow\downarrow} + G^{\downarrow\uparrow}$ describing injection and collection of both spin-species in the device of Fig. 1. Disorder-averaging is performed over the same ensemble of samples studied in Fig. 3. Antilocalization effects $G_X, G_Y, G_Z > G_0$ are substantial (destroying Anderson insulator formed for $W \gtrsim 6$) at strong Rashba SO coupling $t_{\text{so}}^{\text{R}} = 1.0$, much smaller for $t_{\text{so}}^{\text{R}} = 0.1$, and virtually gone at $t_{\text{so}}^{\text{R}} = 0.01$.

conductances G_X, G_Y , and G_Z . For example, $G \equiv G_Z$ means that the spin part, $|\uparrow\rangle$ or $|\downarrow\rangle$, of the asymptotic scattering state (4) is an eigenstate of $\hat{\sigma}_z$, i.e., fully polarized along the z -axis. They should be contrasted with $\text{Var}G_0$ in Fig. 2. Comparison is facilitated by looking at the reduction factor $\text{Var}G_0/\text{Var}G$ in Fig. 4, which also depends on the direction of magnetization of the ferromagnetic contacts (i.e., chosen spin-polarization axis). This is due to the breaking of rotational invariance by the Rashba term (whose electric field always lies along the z -axis). While G_X and G_Z (characterizing the device having magnetization of the leads in the plane orthogonal to the direction of virtual Rashba magnetic field) are similar and exhibit a similar pattern of CF as a function of disorder strength, the two setups can still be distinguished by looking at the CF patterns of partial conductances that are summed in Eq. (19) to get full conductances for unpolarized transport.

Further inspection of the total conductances in Fig. 5 shows that below $W \simeq 2$, the system is in the quasiballistic transport regime ($\ell \gtrsim L$) where $G_0 > G_X, G_Y, G_Z$ because of the additional scattering at the FM-Sm interface which can arise due to band structure mismatch³⁵ induced by the Rashba term. Upon entering the diffusive regime antilocalization $G_0 < G_Z, G_Y, G_Z$ sets in as a standard quantum-interference effect (which survives disorder averaging) pertinent to all spin-orbit interactions affecting phase-coherent propagation through disorder.^{14,50} Thus, strong SO coupling impedes localization effects on both the CF and conductances, even at very high disorder. At smaller SO couplings in Fig. 5, the antilocalization effects are substantially diminished ($t_{\text{so}}^{\text{R}} = 0.1$) or vanish $G_0 \approx G_X, G_Y, G_Z$ altogether ($t_{\text{so}}^{\text{R}} = 0.01$). Nevertheless, the presence of weak SO coupling (i.e., small $t_{\text{so}}^{\text{R}}/W$) is still palpable in the CF plotted in Fig. 4, and even more so in the relationship between different partial conductances studied in Sec. IV.

IV. SPIN-RESOLVED PARTIAL CONDUCTANCES IN DISORDERED RASHBA SPIN-SPLIT ELECTRON SYSTEM

The long lifetime of the electron spin orientation has lead to plausible expectations that the conductance of a two-terminal device $G^{\uparrow\uparrow}$ with parallel magnetizations in the ferromagnetic contacts should be higher than $G^{\uparrow\downarrow}$ when that orientation is antiparallel.^{2,6} However, a recent experiment²⁶ has unraveled surprising result for the disorder-averaged conductance difference ($G^{\uparrow\uparrow} - G^{\uparrow\downarrow}$): it decreases upon increasing sample length (InAs containing 2DEG that is attached to permalloy leads), and eventually turns negative in the quasiballistic transport regime $\ell \sim L$. Theoretical modeling⁴ of the effect of localized spin-flip interactions, which couple two spin subsystems at a discrete sets of points within a mesoscopic disordered sample, finds similar phenomenon under the simplified assumptions for quantum-mechanical transmissiv-

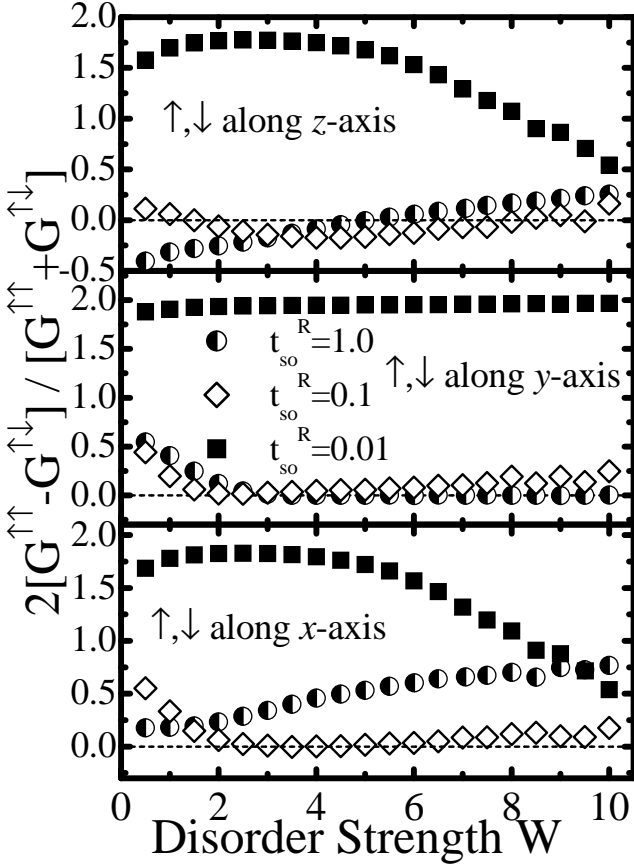


FIG. 6: Disorder-averaged relative conductance difference $\Delta G_{\uparrow\downarrow}^{\uparrow\uparrow}/G_{\uparrow\downarrow}^{\uparrow\uparrow}$ as functions of the disorder strength (i.e., in different transport regimes: ballistic, quasiballistic, diffusive, and localized), Rashba SO coupling, and the direction of magnetization in the leads with respect to the z -axis Rashba electric field. The injected electrons, into the same set of Rashba spin-split disordered conductors studied in Fig. 3, are spin-up polarized in the direction denoted on each panel.

ities (e.g., $T^{\uparrow\downarrow}$) that are independent of the spin orientation of the incoming electron. The results of Sec. III point out that such a treatment is not sufficient in devices with a Rashba SO coupling (as hinted at in Ref. 4). Therefore, we analyze in Fig. 6 the disorder-averaged conductance differences (normalized by respective sums) when an \uparrow -electron is injected

$$\frac{\Delta G_{\uparrow\downarrow}^{\uparrow\uparrow}}{G_{\uparrow\downarrow}^{\uparrow\uparrow}} = 2 \frac{\langle G^{\uparrow\uparrow} - G^{\uparrow\downarrow} \rangle}{\langle G^{\uparrow\uparrow} + G^{\uparrow\downarrow} \rangle}, \quad (20)$$

while Fig. 7 plots the corresponding differences for injection of a spin-down electron

$$\frac{\Delta G_{\uparrow\downarrow}^{\downarrow\downarrow}}{G_{\uparrow\downarrow}^{\downarrow\downarrow}} = 2 \frac{\langle G^{\downarrow\downarrow} - G^{\downarrow\uparrow} \rangle}{\langle G^{\downarrow\downarrow} + G^{\downarrow\uparrow} \rangle}, \quad (21)$$

using three different cases for the spin-polarizations of incoming electron with respect to the z -axis Rashba electric field. The set of disorder and SO hopping param-

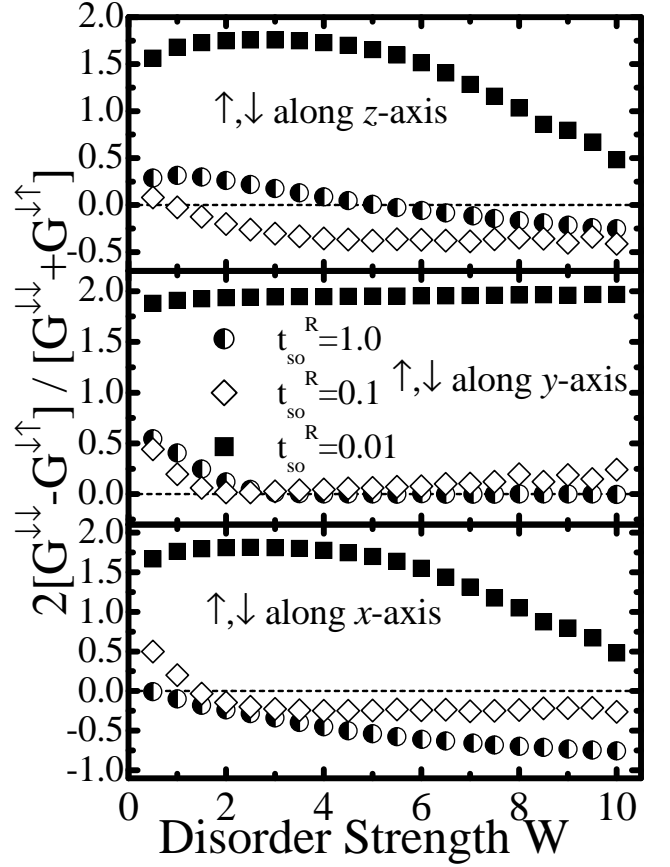


FIG. 7: Disorder-averaged relative conductance difference $\Delta G_{\uparrow\downarrow}^{\downarrow\downarrow}/G_{\uparrow\downarrow}^{\downarrow\downarrow}$ as functions of the disorder strength, Rashba SO coupling, and the orientation of magnetization in the leads with respect to the z -axis Rashba electric field. The injected electrons, into the same set of Rashba spin-split disordered conductors studied in Fig. 3, are spin-down polarized in the direction denoted on each panel.

ters is the same as in Sec. III. Comparing $\Delta G_{\uparrow\downarrow}^{\uparrow\uparrow}/G_{\uparrow\downarrow}^{\uparrow\uparrow}$ and $\Delta G_{\uparrow\downarrow}^{\downarrow\downarrow}/G_{\uparrow\downarrow}^{\downarrow\downarrow}$ shows that the relationship between conductances for parallel and antiparallel magnetization in the leads is quite intricate: for the x -axis or z -axis magnetization, the Rashba spin-split system is not invariant with respect to the spin-subsystem interchange; on the other hand, in the case of polarization along the y -axis invariance holds, $\Delta G_{\uparrow\downarrow}^{\uparrow\uparrow}/G_{\uparrow\downarrow}^{\uparrow\uparrow} \approx \Delta G_{\uparrow\downarrow}^{\downarrow\downarrow}/G_{\uparrow\downarrow}^{\downarrow\downarrow}$. We also find that some of the conductance differences for the x - and y -polarization direction can change sign, even for small SO coupling ($t_{so}^R/W \sim 0.1$). This occurs within different transport regimes, depending on the polarization of the incoming electron, so that negative values of conductance differences are not confined only to the quasiballistic transport regime as in Refs. 4,26 (the most similar case here to their phenomenology is \uparrow polarized, along the z -axis, current injected into the conductor with moderate SO coupling $t_{so}^R = 0.1$).

These negative values for conductance differences in 2D mesoscopic spintronics disordered systems is a mani-

festation of a novel quantum interference effect involving the two spin components.⁴ For instance, if an \uparrow -electron is injected into a ballistic sample, the Rashba interaction will induce spin precession rendering non-zero $G^{\uparrow\downarrow} \neq 0$ because the \downarrow -electron could be detected at the drain even if no spin-down electrons are injected at the source.^{2,11} When scattering off impurities is added to the SO interaction, the injected electron pure quantum state, with definite spin and momentum, evolves into another pure quantum state that is a linear superposition (as discussed in Sec. II) of different and entangled momentum and spin eigenstates. In the intuitive (semiclassical) picture of Feynman paths,²⁶ for some device configurations shown in Figs. 6 and 7, this superposition is equivalent to a destructive interference taking place along those trajectories where projection of the electron spin on the magnetization axis of the source has not yet changed sign at the drain contact.

V. CONCLUSION

Using our efficient real \otimes spin space formalism for the evaluation of partial spin-resolved conductances, expressed in terms of a Landauer-type formula, we have investigated some of the standard interference effects in the quantum-coherent propagation of electrons through two-dimensional disordered conductor, which is attached to two ferromagnetic contacts and is exposed to a Rashba spin-orbit coupling. In the limit of a strong Rashba interaction, all computed conductances exhibit a critical value of $\simeq e^2/h$ in a substantial interval of large disorder, where G_0 for the time-reversal and spin-rotation invariant system is negligible because of strong localization effects. The freezing out of the fluctuations of the total conductances, $\text{Var } G_X$, $\text{Var } G_Y$, and $\text{Var } G_Z$, is even more dramatic, in contrast to the pure disordered case where the CF decay exponentially fast. The impediment of the Anderson localization at strong disorder resembles a weak-antilocalization effect due to SO scattering off impurities,¹⁴ which is known to generate a metal-insulator transition in 2D systems (otherwise,

they are Anderson insulators, albeit with an exponentially large ξ at weak disorder³¹). Nevertheless, it has been known that the Rashba induced antilocalization can be considerably different^{50,51} from the standard weak-antilocalization expression of Ref. 14. While both conductance fluctuations and localization effects are thought to fall into three universality classes (determined only by the invariance properties of the Hamiltonian of a conductor with respect to time-reversal and spin-rotation symmetry operations¹⁰), here we demonstrate how the tracking of individual spin subsystems (i.e., injection and detection of spin-polarized electrons) allows one to reveal non-universal features specific to the Rashba SO coupling effects on the phase-coherent propagation through disorder. For example, one has to take into account the angle between the spin-polarization of an incoming electron and the Rashba electric field. Moreover, the relationship between spin-resolved partial conductances unearths additional quantum interference effects specific to the context of spintronics: for particular set of disorder, SO, and spin-polarization parameters, one can obtain special superpositions of the two spin components, which, being entangled with orbital states of mesoscopic disordered systems, generate higher conductance for the two-terminal device with antiparallel contact magnetization than for parallel configuration.

Finally, we emphasize that our findings are *numerically exact* within the single-particle picture of transport, and therefore non-perturbative in both the strength of the disorder³³ and SO interaction¹¹. For example, at large enough W the concept of mean free path, which is relevant for semiclassical transport and perturbative quantum interference corrections to it, ceases to exist³³ ($\ell < a \lesssim \lambda_F$). Eventually, the localized phase is encountered when $L \gg \xi$.

Acknowledgments

We thank E. I. Rashba, J. Fabian, D. Frustaglia, and I. Žutić for enlightening discussions. This work was supported in part by ONR grant N00014-99-1-0328.

* Present address: Department of Physics and Astronomy, University of Delaware, Newark, DE 19716-2570

¹ S. A. Wolf, D. D. Awschalom, R. A. Buhrman, J. M. Daughton, S. von Molnár, M. L. Roukes, A. Y. Chtchelkanova, and D. M. Treger, *Science* **294**, 1488 (2001); S. Das Sarma, J. Fabian, X. Hu, and I. Žutić, *Solid State Commun.* **119**, 207 (2001).

² S. Datta and B. Das, *Appl. Phys. Lett.* **56**, 665 (1990).

³ G. Burkard, H.-A. Engel, and D. Loss, *Fortschr. Phys.* **48**, 9-11, 965 (2000).

⁴ P. Šeba, P. Exner, K.N. Pichugin, A. Vyhnal, and P. Štředa, *Phys. Rev. Lett.* **86**, 1598 (2001).

⁵ G. Schmidt, D. Ferrand, L.W. Molenkamp, A.T. Filip, and

B.J. van Wees, *Phys. Rev. B* **62**, R4790 (2000).

⁶ M. Johnson, *Phys. Rev. B* **58**, 9635 (1998); M. Johnson and R. Silsbee, *Phys. Rev. B* **37**, 5326 (1988).

⁷ *Mesoscopic Phenomena in Solids*, edited by B.L. Altshuler, P.A. Lee, and R.A. Webb (North-Holland, Amsterdam, 1991).

⁸ S. Yuasa, T. Nagahama, and Y. Suzuki, *Science* **297**, 234 (2002).

⁹ S. Datta, *Electronic Transport in Mesoscopic Systems* (Cambridge University Press, Cambridge, 1995).

¹⁰ C.W.J. Beenakker, *Rev. Mod. Phys.* **69**, 731 (1997).

¹¹ F. Mireles and G. Kirczenow, *Phys. Rev. B* **64**, 024426 (2001); F. Mireles and G. Kirczenow, *Europhys. Lett.* **59**,

- 107 (2002).
- ¹² G. Feve, W. D. Oliver, M. Aranzana, and Y. Yamamoto, Phys. Rev. B **66**, 155328 (2002).
- ¹³ E.I. Rashba, Fiz. Tverd. Tela **2**, 1224 (1960) [Sov. Phys.-Solid State **2**, 1109 (1960)].
- ¹⁴ S. Hikami, A.I. Larkin, and Y. Nagaoka, Prog. Theor. Phys. **63**, 707 (1980).
- ¹⁵ J. Nitta, T. Akazaki, H. Takayanagi, and T. Enoki, Phys. Rev. Lett. **78**, 1335 (1997).
- ¹⁶ A. Fert and H. Jaffrès, Phys. Rev. B **64**, 184420 (2001); E.I. Rashba, Eur. Phys. J. B **29**, 513 (2002).
- ¹⁷ F. F. Jedema, A. T. Filip, and B. J. van Wees, Nature (London) **410**, 345 (2001).
- ¹⁸ J. A. C. Bland, A. Hirohata, C. M. Guertler, Y. B. Xu and M. Tselepi, J. Appl. Phys. **89**, 6740 (2001); P. R. Hammar and M. Johnson, Phys. Rev. Lett. **88**, 066806 (2002); R. M. Potok, J. A. Folk, C. M. Marcus, V. Umansky, Phys. Rev. Lett. **89**, 266602 (2002).
- ¹⁹ T. Matsuyama, C.-M. Hu, D. Grundler, G. Meier, and U. Merkt, Phys. Rev. B **65**, 155322 (2002).
- ²⁰ J. Schliemann, J. Carlos Egues, and D. Loss, cond-mat/0211603.
- ²¹ J. M. Kikkawa and D. D. Awschalom, Nature (London) **397**, 139 (1999).
- ²² J. M. Kikkawa and D. D. Awschalom, Phys. Rev. Lett. **80**, 4313 (1998).
- ²³ J. Fabian and S. Das Sarma, J. Vac. Sc. Technol. B **17**, 1708 (1999).
- ²⁴ J. Nitta, F. Meijer, and H. Takayanagi, Appl. Phys. Lett. **75**, 695 (1999).
- ²⁵ J. B. Miller, D. M. Zumbuhl, C. M. Marcus, Y. B. Lyanda-Geller, D. Goldhaber-Gordon, K. Campman, A. C. Gosard, cond-mat/0206375.
- ²⁶ C.-M. Hu, J. Nitta, A. Jensen, J.B. Hansen, and H. Takayanagi, Phys. Rev. B **63**, 125333 (2001).
- ²⁷ L.E. Ballentine, *Quantum Mechanics: A Modern Development* (World Scientific, Singapore, 1998).
- ²⁸ B. K. Nikolić, cond-mat 0301614.
- ²⁹ D. Giulini, E. Joos, C. Kiefer, J. Kupsch, I.-O. Stamatescu, and H. D. Zeh, *Decoherence and the appearance of a classical world in quantum theory*, (Springer-Verlag, Heidelberg, 1996).
- ³⁰ J. König and Y. Gefen, Phys. Rev. Lett. **86**, 3855 (2001).
- ³¹ J.A. Vergés, Phys. Rev. B **57**, 870 (1998).
- ³² P.A. Lee, A.D. Stone, and H. Fukuyama, Phys. Rev. B **35**, 1039 (1987).
- ³³ B.K. Nikolić and P.B. Allen, Phys. Rev. B **63**, R020201 (2001).
- ³⁴ Y. Imry and R. Landauer, Rev. Mode. Phys. **71**, S306 (1999).
- ³⁵ B.K. Nikolić and P.B. Allen, J. Phys.: Condens. Matter **12**, 9629 (2000).
- ³⁶ M. Johnson and R.H. Silsbee, Phys. Rev. Lett. **55**, 1790 (1985).
- ³⁷ H. Ohno, Science **281**, 951 (1998).
- ³⁸ M.A.M. Gijs and G.E.W. Bauer, Adv. Phys. **46**, 286 (1997), and references therein.
- ³⁹ A. Brataas, Yu.V. Nazarov, and G.E.W. Bauer, Phys. Rev. Lett. **84**, 2481 (2000).
- ⁴⁰ B.I. Halperin, A. Stern, Y. Oreg, J.N.H.J. Cremers, J.A. Folk, and C.M. Marcus, Phys. Rev. Lett. **86**, 2106 (2001).
- ⁴¹ M.I. D'yakonov and V.I. Perel', Sov. Phys. JETP **33**, 1053 (1971).
- ⁴² C. Caroli, R. Combescot, P. Nozieres, and D. Saint-James, J. Phys C **4**, 916 (1971).
- ⁴³ Y. Meir and N.S. Wingreen, Phys. Rev. Lett. **68**, 2512 (1992).
- ⁴⁴ C.P. Umbach, S. Washburn, R.B. Laibowitz, and R.A. Webb, Phys. Rev. B **30**, 4048 (1984); R.A. Webb in Ref. 7.
- ⁴⁵ B.L. Altshuler, Pis'ma Zh. Eksp. Theor. Fiz. **41** (1985) [JETP Lett. **41**, 648 (1985)].
- ⁴⁶ Y. Asano and G.E.W. Bauer, Physica B **249-251**, 523 (1998).
- ⁴⁷ J.A. Folk, S.R. Patel, K.M. Birnbaum, C.M. Marcus, C.I. Duruöz, and J.S. Harris, Jr., Phys. Rev. Lett. **86**, 2102 (2001).
- ⁴⁸ I.L. Aleiner and V.I. Fal'ko, Phys. Rev. Lett. **87**, 256801 (2001).
- ⁴⁹ The largest experimentally observed value of the Rashba SO coupling is $\alpha_R = 3 \cdot 10^{-12}$ eV m in InAs-based heterojunctions.¹⁵ There seems to be no fundamental obstacle in making it larger through a proper choice of material, geometry, and external gates.
- ⁵⁰ S.V. Iordanskii, Yu.B. Lyanda-Geller, and G.E. Pikus, JETP Letters **60**, 206 (1994).
- ⁵¹ G.L. Chen, J. Han, T.T. Huang, S. Datta, and D.B. Janes, Phys. Rev. B **47**, R4084 (1993).